Negative thermal expansion of the stars of David in a 1*T*-$NbSe_2$ monolayer at about 50 K

Li Cheng,[1,2] Chen Liang,[1] Xiaolong Zou,[1] Zheng Liu,[2] Jian Wu,[3,4,*] Shunhong Zhang,[5,†] and Shuang Qiao[6,7,‡]

[1]*Shenzhen Geim Graphene Center (SGC), Tsinghua-Berkeley Shenzhen Institute (TBSI) and Tsinghua Shenzhen International Graduate School, Tsinghua University, Shenzhen 518055, People's Republic of China*

[2]*Institute for Advanced Study, Tsinghua University, Beijing 100084, People's Republic of China*

[3]*State Key Laboratory of Low Dimensional Quantum Physics, Department of Physics, Tsinghua University, Beijing 100084, People's Republic of China*

[4]*Frontier Science Center for Quantum Information, Beijing 100084, People's Republic of China*

[5]*International Center for Quantum Design of Functional Materials (ICQD), University of Science and Technology of China, Hefei 230026, Anhui, People's Republic of China*

[6]*Department of Physics, Capital Normal University, Beijing 100048, People's Republic of China*

[7]*Beijing Computational Science Research Center, Beijing 100193, People's Republic of China*

(Received 8 November 2022; revised 7 September 2023; accepted 22 September 2023; published 12 December 2023)

1*T*-$NbSe_2$ is a d^1 transition metal dichalcogenide, featuring a low-*T* $\sqrt{13} \times \sqrt{13}$ commensurate charge-density-wave (CCDW) phase with the formation of a star of David (SD) pattern. Here, we investigate the temperature dependence of the lattice and electronic structures of the 1*T*-$NbSe_2$ monolayer using *ab initio* molecular dynamics simulations, which predicts that the CCDW phase transition can persist up to 350 K. Before melting, an unprecedented enhancement of CCDW order is revealed at ∼50 K, characterized by two order parameters which respectively indicate the in-plane negative thermal expansion and out-of-plane buckling of the SDs. Such lattice distortion takes place in each SD individually via a detailed balance kinetic process, and the induced sharp variation of the charge gap size and the local density of states are consistent with recent scanning tunneling microscopy observations. This unique phenomenon, which is absent in the more extensively studied d^1 transition metal dichalcogenide 1*T*-TaS_2, is explained by the delicate competition between lattice energy and entropy.

DOI: 10.1103/PhysRevB.108.214103

I. INTRODUCTION

The charge density wave (CDW) transitions in layered d^1 transition metal dichalcogenides (TMDs), such as TaS_2, $TaSe_2$, and $NbSe_2$, have long been studied [1–14]. The intimate connection between the CDW and Mott physics in the 1*T* polymorph of these materials endows them with rich and tunable electronic phases, which is not only fundamentally intriguing but also highly desirable for applications such as ionic field-effect transistors [4] and ultrafast switches and memories [15–17]. More importantly, these 1*T*-TMDs have recently received revived interest due to the prospect of hosting the exotic quantum spin-liquid (QSL) state [14,18–25], which also relies on the Mott localization of the d^1 electron in a star of David (SD) geometry subject to a commensurate CDW (CCDW) order.

$NbSe_2$ in the natural bulk form was known to exist in the 2*H* phase only [26]. The low-energy physics of this phase in the monolayer limit is governed by a single metallic *d* band, whose interplay with phonons and spin-orbit coupling gives rise to rich exotic quantum phenomena including CDW [27], Ising superconductivity [28], and magnetic instability [29]. On the other hand, the 1*T* polymorph of $NbSe_2$ had long been absent until the advances of molecular beam epitaxial techniques enabled its controllable growth of the monolayer [30]. Bearing close resemblance to 1*T*-TaS_2 in both crystal and electronic structures while exempted from undesired stacking complexity, 1*T*-$NbSe_2$ has drawn tremendous interest [9,30–33]. In stark contrast with its metallic 2*H* counterpart, both scanning tunneling spectroscopy (STS) and angle-resolved photoemission spectroscopy revealed an insulating gap [9,30–33] in 1*T*-$NbSe_2$ within the CCDW regime, which can be unambiguously attributed to the d^1 Mott physics. More interestingly, an obvious change of the scanning tunneling microscopy (STM) topographic image was observed at ∼50 K [33], much lower than the CCDW melting temperature, indicating an extra transition of the structural or electronic phase. Under positive bias, the SDs undergo a dark-to-bright transition when the temperature is elevated from 4.4 to 77 K, accompanied with an emergent peak in the high-temperature STS spectra [33]. With the aid of *ab initio* molecular dynamics (AIMD) performed at 50 K, a unique modulation to the low-temperature CCDW lattice structure, featuring shrinkage of SDs, is identified, and the resultant downward shift of upper Hubbard band consistently interprets the observed lightening of SDs and onset of in-gap states [33].

*wu@tsinghua.edu.cn
†szhang2@ustc.edu.cn
‡6972@cnu.edu.cn

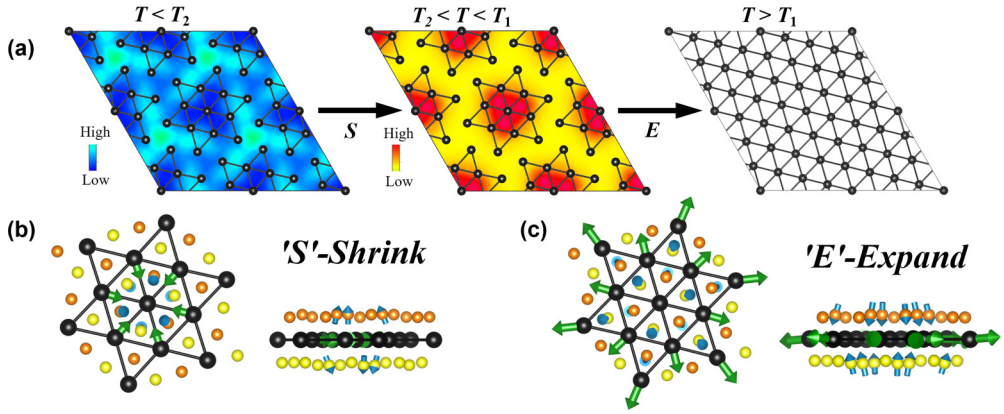

FIG. 1. (a) Schematics of the phase transitions in the $1T$-$NbSe_2$ monolayer. For clarity, only the Nb atoms are shown from top view. The coloring mappings in the left and central panels show the simulated scanning tunneling microscopy (STM) topography of low buckled structure (LBS) and high buckled structure (HBS) at $V_b = 0.36$V, both in the commensurate charge density wave (CCDW) regime but contains dark and bright stars of David (SDs), respectively (the High end of the color bar represents the bright region in topographies). Lattice distortion associated with (b) the negative thermal expansion (NTE) phase transition across T_2 (LBS-to-HBS) and (c) the CCDW transition across T_1, with the arrows indicating the atomic displacements. The LBS structure is obtained by the DFT + U relaxation, while the HBS and high-symmetric phase structure are the ensemble-averaged equilibrium crystal structures from *ab initio* molecular dynamics (AIMD) simulations at ∼50 and 400 K, respectively.

In this paper, the AIMD simulation is extended from a single temperature point (50 K) to 16 temperature points covering the range between 5 and 600 K. By closely tracing the thermal evolution of the CCDW order parameter, we construct the phase diagram of the $1T$-$NbSe_2$ monolayer from first-principles calculations. Two distinct CCDW phases differentiated by a first-order transition ∼50 K are clearly revealed. We show that this transition uniquely features negative thermal expansion (NTE) of the SDs. The physical origin is attributed to the competition between the internal energy and lattice entropy.

II. METHODS

Our AIMD simulations and first-principles calculations based on density functional theory (DFT) are performed by using VASP [34–39], with most setups following our previous AIMD study on $1T$-TaS_2 [40]. The correlation effects of Nb-4d electrons are treated by a simplified rotationally invariant DFT + U correction which depends on a single parameter $U_{\text{eff}} = U - J$. The on-site Coulomb repulsion U has a value of ∼3.0 eV as obtained via the linear response approach in earlier works [7,41], while the Hund's coupling J is supposed to be smaller given the d^1 configuration of Nb. We thereby use $U_{\text{eff}} = 3.0$ eV, which in the AIMD simulations predicts NTE transition temperature falling into the interval estimated from STS spectra variation [33]. Detailed testing results quantifying the influence of U_{eff} values on the lattice structures are summarized in Table S1 in the Supplemental Material [42]. It is also found that the + U correction is crucial for obtaining the correct spin-polarized electronic structure in the CCDW phase (Fig. S1 in the Supplemental Material [42]). We use the DFT + U linear response method implemented in VASP to calculate the dynamic matrix and use the PHONOPY package [43] to compute the phonon properties.

With the lattice constants fixed to the experimental value [7,33], the in-plane stress tensors (XX or YY) for the high-symmetric phase and the two CCDW phase (lower and higher temperature) are calculated to be 15.5, 15.8, and 13.6 kBar, respectively. Such a small difference of stress tensor suggests that the change of lattice constants should be rather small across the NTE transition given that the strain has been released by the local distortion of SDs. Indeed, our experimental collaborators [33] did not observe visible change of lattice constants when temperature varies across the dark-to-bright transition point. Thus, we fixed lattice constants to the experimental value through our simulations. We relax the atomic positions from the high-symmetric phase [Fig. 1(a), right panel] with standard DFT + U calculations within a $\sqrt{13} \times \sqrt{13}$ supercell using a $4 \times 4 \times 1$ Γ-centered uniform k-mesh, yielding a CCDW phase with one SD. An enlarged $2\sqrt{13} \times 2\sqrt{13}$ supercell is then constructed for AIMD simulations, with the folded Brillouin zone represented by a single Γ point. To simulate the structure evolution of the monolayer upon elevated temperature, the canonical ensemble is implemented, with the thermal bath realized by a Nosé thermostat. Starting from 5 K, we increase the temperature iteratively and progressively, by using the final structure of low temperature as the initial structure of the next higher temperature. The thermal equilibrium of the lattice structure is carefully ensured at each target temperature, which is asserted based on two criteria: (a) according to the Boltzmann distribution, the temperature fluctuation has been $<\sqrt{(0.67 * N_{\text{tot}})}$ (N_{tot} is the number of atoms in the supercell), and (b) atoms have vibrated periodically with constant amplitude. Based on careful tests, a timestep of 2 fs and a total duration of 20 ps are adopted for the AIMD simulation of each temperature, in which the thermal equilibrium can been guaranteed during the last 4 ps, and accordingly, the thermodynamic properties (e.g., the equilibrium crystal structure) are accessed by sampling snapshot configurations. The capability of AIMD simulations in predicting CDW transitions of layered materials has been demonstrated in our earlier work on $1T$-TaS_2 [40] and some works from other groups [44,45].

III. RESULTS

A. NTE phase transition before CCDW melting

The $1T$-$NbSe_2$ monolayer consists of a triangular lattice of Nb atomic layer sandwiched by two Se layers. The label T denotes a local $NbSe_6$ octahedral coordination, as commonly adopted in most layered TMDs to distinguish it from the trigonal prismatic $2H$ phase. This high-symmetric phase can only survive at high temperature, possessing a uniform triangular Nb lattice [Fig. 1(a), right panel] with all Nb atoms symmetrically equivalent and evenly spaced by $d_0 \sim 3.46$ Å. At low temperature, a $\sqrt{13} \times \sqrt{13}$ supercell spontaneously forms, in which the 13 Nb atoms form a SD [Fig. 1(a), left and central panels], like the well-studied CCDW phase of $1T$-TaS_2. Within a SD, the 13 Nb atoms can be grouped into three inequivalent classes: one at the center of the SD (Nb^C), six nearest to the Nb^C (Nb^N), and the remaining six at the edge of the SD (Nb^E). The CCDW transition reduces the Nb^C–Nb^N distance (d_{CN}) to ~3.26 Å. We define $\Delta_{CDW} = d_0 - d_{CN}$, sketched in the top panels of Figs. 2(a) and 2(b), as an order parameter, based on which the CCDW transition can be closely tracked.

Figure 2(c) shows the evolution of Δ_{CDW} corresponding to one of the four SDs, as a function of temperature, which clearly shows two kinks. This is quite different from our previous AIMD study on $1T$-TaS_2, wherein we observed Δ_{CDW} decreased gradually and mildly before collapsing at the melting temperature [40]. In Fig. 2(c), the kink at $T_1 \sim$ 350 K signifies the CCDW melting temperature. As a reference, the CCDW transition temperature of $1T$-TaS_2 has been estimated to be ~300 K by using the same method [40], nicely consistent with the experimental value. The kink at $T_2 \sim 50$ K, however, is uniquely present in the Δ_{CDW}-T profile of $1T$-$NbSe_2$. More interestingly, Δ_{CDW} increases as the temperature is elevated, namely, the SDs contract toward their centers. On the other hand, T_2 is quite close to the onset temperature of the in-gap state in the experimental conductance spectra. These facts indicate that the experimentally observed dark-to-bright transition of SDs [33] essentially corresponds to an unusual thermal enhancement of CCDW order.

To visualize the structure evolution across T_2 and elucidate the underlying mechanism of such a NTE phase transition, we compare the thermally equilibrated atomic structures of $1T$-$NbSe_2$ below and above T_2. As contrasted in Figs. 1(a) and 1(b), the NTE of SDs mainly involves the Nb^N atoms and the Se atoms nearest to Nb^C (Se_1). The most significant distortion takes place on the Nb^N atoms, which displace inward along the in-plane Nb^N–Nb^C direction. Such a distortion in turn pushes Se_1 away from the Nb layer along the out-of-plane direction, accompanied by a slight in-plane displacement toward the center of the SD. Thus, the NTE transition can also be characterized by the vertical height of the Se_1 atoms relative to the central Nb plane, as illustrated in the bottom panels of Figs. 2(a) and 2(b). The change of this variable $h_{CDW} = h_{Se1} - h_0$ ($h_0 \sim 1.71$ Å is the value of h_{Se1} in the high-temperature phase) can be defined as another CCDW order parameter which, as is also plotted in Fig. 2(c), consistently characterizes two transitions at T_1 and T_2. We hereafter term the structure below T_2 with smaller h_{CDW} as the low buckled structure (LBS) and the one between T_2 and T_1 as the high buckled structure (HBS); the ensemble-averaged atomic coordinates of both structures can be found in the Supplemental Material Note B [42]. We also simulate their STM images, as shown in Fig. 1(a), yielding nice agreement with the experimentally observed distinct topographies at 4.4 and 77 K, featured by dark and bright SDs respectively [33]. Effects of NTE on the Mott physics can be found in Supplemental Material Note C [42]; the electronic structure changes are due to the strength varying of the hybridization between the Nb^C-d_{z^2} and Se_1-p orbitals. The p-d hybridization is weaker/stronger in LBS/HBS state.

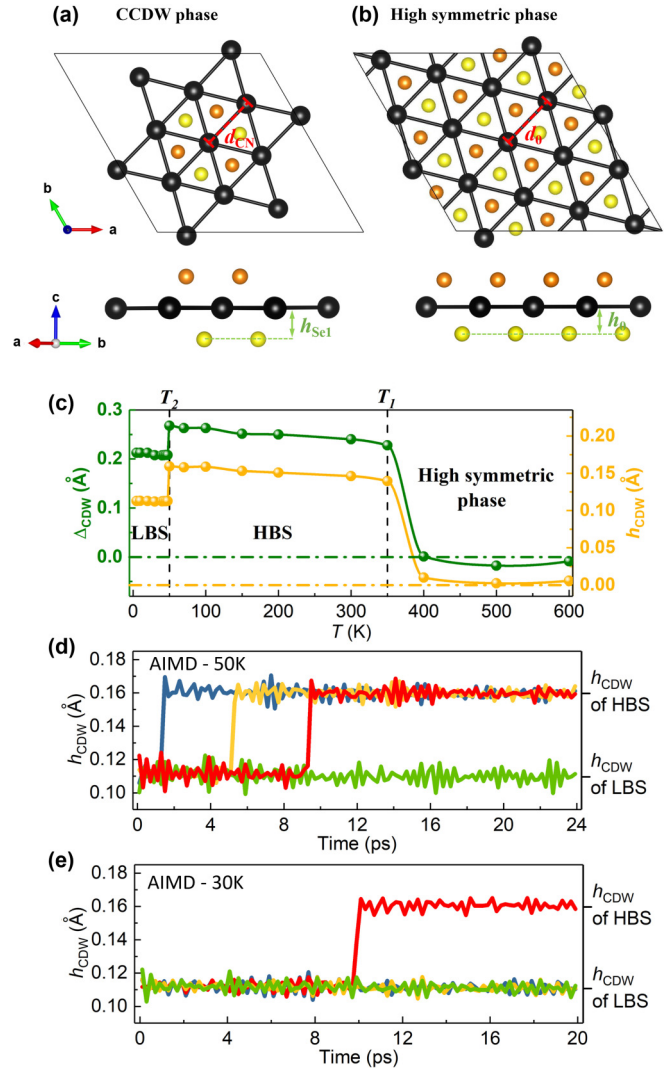

FIG. 2. (a) and (b) Definition of the commensurate charge density wave (CCDW) order parameter Δ_{CDW} ($\Delta_{CDW} = d_0 - d_{CN}$) and h_{CDW} ($h_{CDW} = h_{Se1} - h_0$) in $1T$-$NbSe_2$. (c) Temperature-dependent Δ_{CDW} and h_{CDW} of a representative star of David (SD) extracted from *ab initio* molecular dynamics (AIMD) simulations. Horizontal and vertical lines denote zeroes of the order parameters and the transition temperature, respectively. (d) and (e) Evolution of SD-resolved h_{CDW} from two individual simulations at (d) 50 K and (e) 30 K, within a supercell initially containing four low buckled structure (LBS) SDs. Each colored curve represents a specific SD, and the abrupt increase indicates its negative thermal expansion, namely, a local LBS-to-high buckled structure (HBS) transition.

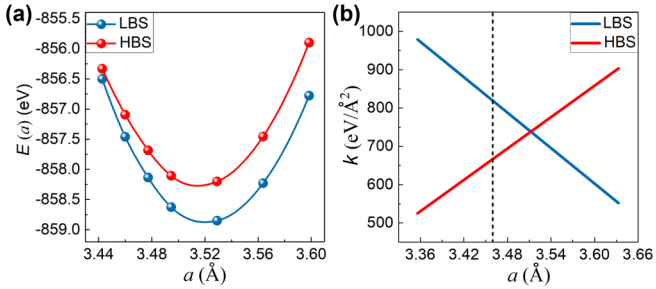

FIG. 3. (a) Static total energy E of the low buckled structure (LBS) and high buckled structure (HBS) as a function of lattice constants a, obtained from DFT + U calculations. (b) Elastic constant k obtaining by fitting the E-a curves. The dash line labels the experimental lattice constant a_0.

Going beyond the thermodynamics, we also trace the kinetics of the NTE transition. Figure 2(d) shows the temporal evolution of the SD-resolved h_{CDW} at $T = 50$ K starting from the LBS configuration. During the simulated heating process, a series of local LBS-to-HBS transitions takes place individually and consecutively in three SDs, while the last SD stays in the LBS. If heated at a relatively lower temperature $T = 30$ K, it takes longer to observe the first local LBS-to-HBS transition, and 3 of the 4 SDs stay in the LBS state for >20 ps [Fig. 2(e)]. These simulation results are consistent with the partial brightening of SDs observed experimentally [33] and imply that the thermally driven structural distortion could originate from competition and detailed balance between the internal energy and lattice entropy rather than softening of specific phonon mode. Combining Figs. 2(c)–2(e), one can infer that the LBS-to-HBS transition for each individual SD is locally of first-order feature, although the exact occurring temperature can vary from one SD to another. Indeed, our simulation indicates that a higher temperature of 70 K is necessary to accomplish LBS-to-HBS transition of all four SDs within the simulated duration of 20 ps. Due to the limited computational resources, it is impractical to simulate an ultra-large supercell and perform statistical analysis on a considerable number of SDs. Notwithstanding, we can arguably suggest $T_2 \sim 50$ K as the characteristic temperature of the LBS-to-HBS transition, given the consecutive local transitions observed in our simulations and the quantitative consistency with experiments.

B. Microscopic mechanism of the NTE transition

The thermally triggered LBS-to-HBS transition implies the important role of lattice entropy. At finite temperature, the relative stability of the LBS and HBS can be ascertained based on the free energy $\Delta F = F(\mathrm{LBS}) - F(\mathrm{HBS}) = \Delta E - T\Delta S$. At $T = 0$ K, it reduces to the first-principles total energy, which is calculated to be $\Delta F = \Delta E = -1.7$ meV/atom < 0. The total energy curves of both structures as a function of the lattice constant a are shown in Fig. 3(a), where one can see that $\Delta E < 0$ in a wide range of a, indicating that the overall binding is stronger in the LBS. The curves can be fitted by using a cubic polynomial:

$$E(a) = A + Ba + Ca^2 + Da^3, \tag{1}$$

TABLE I. Parameters obtained by polynomial fitting [Eq. (1)] of the total energy of the 1T-$NbSe_2$ monolayer, with LBS and HBS, respectively, using the lattice constant a as the single variable.

	A	B	C	D
LBS	14 884.4	−12 124.7	3077.0	−257.1
HBS	−6211.3	5852.9	−2029.1	227.6

where the cubic term accounts for some anharmonicity. The coefficients from least-square fitting are listed in Table I. Accordingly, the elastic constant k can be estimated by calculating the second-order derivative d^2E/da^2, which is plotted in Fig. 3(b). Near the experimental lattice constant a_0, the HBS has an elastic constant slightly smaller than that of the LBS, implying its weaker bond strength. Taking an analogy to the Debye model, we can infer that the HBS possesses vibrational modes with overall lower frequency ω, and more modes can be excited at the same temperature. This characteristic typically leads to a larger lattice entropy [$\Delta S = S(\mathrm{LBS}) - S(\mathrm{HBS}) < 0$], namely, at finite temperature, more vibration modes with smaller ω can be excited. Consequently, ΔF has a chance to reverse its sign as the temperature increases ($\Delta E < 0$ and $-T\Delta S > 0$). As a crosscheck of our proposal, we tentatively increase the lattice constant to $a = 3.55$ Å and perform AIMD simulation at 50 K starting from the LBS. In this case, the LBS has an elastic constant slightly smaller than that of the HBS [Fig. 3(b)]; thus, ΔF has no chance to reverse its sign ($\Delta E < 0$ and $-T\Delta S < 0$), and the NTE phase transition is unlikely to occur. Within a simulated heating duration of 20 ps, no LBS-to-HBS transition is observed in the stretched lattice, verifying the soundness of our lattice entropy argument. The local LBS-to-HBS transitions during the AIMD at 30 and 50 K [Figs. 2(d) and 2(e)] can also be viewed as a manifestation of the balance between ΔE and $T\Delta S$.

We further elaborate the mechanism of NTE transition in 1T-$NbSe_2$ by comparing its phononic properties with the isostructural but more extensively studied 1T-TaS_2. Recall that the NTE transition, when firstly revealed experimentally via the dark-to-bright conversion of SDs, was originally attributed to the strong couplings between electrons and two low-energy phonon modes (2.68 and 3.67 THz) corresponding to breathing of SDs [33]. However, our phonon calculations indicate that 1T-TaS_2 also possesses two long-wave breathing modes with similar vibration and frequency (Fig. S3 in the Supplemental Material [42]), yet reports of NTE transition of SDs in its CCDW phase are lacking [40]. The key factor giving rise to such a distinction may lie in a remarkable difference in the vibration spectra of the two isostructural compounds, namely, there is a large phonon gap from 4 to 6 THz in 1T-TaS_2 [Fig. 4(a) vs 4(b)]. Without the phonon gap, a large portion of low-energy modes in the 1T-$NbSe_2$ monolayer can be excited at $T_2 \sim 50$ K, and the accumulated entropy substantially alters the free energy surface, activating the NTE transition. In contrast, the large phonon gap in 1T-TaS_2 impedes excitations of most modes above the gap. Consequently, competing phases with comparable free energy do not exist, and a single phase dominates the whole CCDW

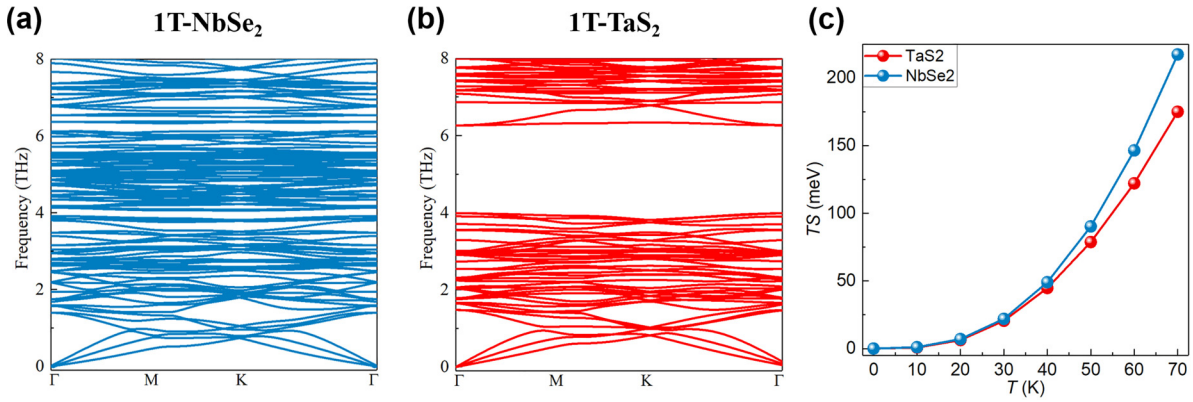

FIG. 4. Calculated phonon spectra of (a) $1T$-$NbSe_2$ [low buckled structure (LBS) state] and (b) $1T$-TaS_2. Phonon bands >8 THz are not shown. (c) Entropy contribution TS of $1T$-$NbSe_2$ and $1T$-TaS_2 to the free energy.

regime. Based on the phonon frequencies of $1T$-$NbSe_2$ and $1T$-TaS_2, we calculate the entropy contribution TS to the free energy as a function of temperature. As shown in Fig. 4(c), the TS of $1T$-$NbSe_2$ becomes larger than that of $1T$-TaS_2 at $T \sim 50$ K, and the difference increases with temperature, also confirming our lattice entropy proposal.

IV. DISCUSSION AND CONCLUSIONS

Figure 5 schematically summarizes the phase diagram of the $1T$-$NbSe_2$ monolayer under varying temperatures, with some characteristic properties qualitatively indicated. When heated from 0 K with progressively elevated temperature, a unique phase transition takes place at $T_2 \sim 50$ K, characterized by NTE of SDs (Δ_{CDW}), namely, the SDs tend to shrink and partially enhance the CCDW order. This phase transition arising from the competition between the lattice energy and

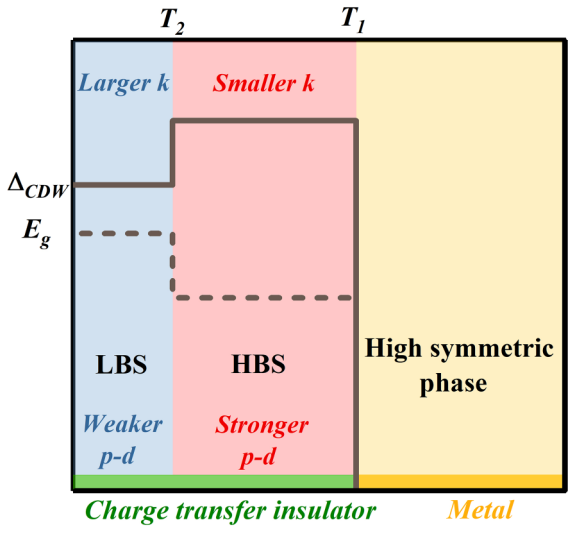

FIG. 5. Schematic phase diagram of $1T$-$NbSe_2$ characterized by both the commensurate charge density wave (CCDW) parameter (Δ_{CDW}), and band gap size (E_g). The region colored by blue (red) corresponds to the dark (bright) stars of David (SDs) observed in experiments. The yellow region represents the high-temperature phase after the CCDW melting.

vibrational entropy distorts the SDs, converting them from LBS to HBS (h_{CDW}), and modulates the Mottness via enhancing the hybridization between the Nb^C-d_{z^2} and Se_1-p orbitals, giving rise to a reduced charge-transfer gap (see Supplemental Material Note C [42] for a detailed discussion) which persists until the HBS-CCDW phase melts at $T_1 \sim 350$ K. The enriched phases in the CCDW regime uniquely present in $1T$-$NbSe_2$ make this d^1 TMD a compelling platform to study the interplay between lattice and charge degrees of freedom. Surrounding the intriguing NTE transition, some open questions could be of general interest to the community. For example, it remains unexplored how the spin state evolves across the transition. At the single-particle level, we have demonstrated in $1T$-TaS_2 that the electron hoppings and band flatness can be efficiently tuned via altering the CDW order strength [46]. In the interacting regime, in this paper, we further reveal the CCDW order enhancement and the accompanied adjustment of correlation strength. Note that the ratio of on-site Coulomb repulsion over the kinetic energy U/t has been elucidated as a key factor in the Hubbard model to mediate rich QSL phases [47]. Some definitive manifestations of such theoretical predictions could be achieved in the $1T$-$NbSe_2$ monolayer. Given the local nature of NTE transition, bright and dark SDs may coexist near T_2, and it would be intriguing to investigate the local morphology and electronic structure of the domain wall separating the LBS and HBS regions with distinct degrees of Mott localization.

In conclusion, we have systematically studied the evolution of the CCDW order of the $1T$-$NbSe_2$ monolayer in a wide temperature range. By performing extensive AIMD simulations and first-principles calculations, we establish renewed understanding on the recently discovered thermally induced dark-to-bright transition. It is found that the transition is of structural origin, and two order parameters are proposed to coherently capture the local distortion: Δ_{CDW} indicates the NTE of SDs, while h_{CDW} depicts the buckling near the SD center. Thermodynamic and kinetic analyses on the AIMD results reveal the local and stochastic feature of the NTE transition, pointing the likely underlying mechanism to the entropic effect. When the temperature is raised to $T_2 \sim 50$ K, the effect of lattice entropy swaps the free energy sequence of LBS and HBS, and the NTE phase transition in the CCDW regime is triggered by thermal perturbation. Noting the remarkable

difference in the vibration spectra between the isostructural $1T$-$NbSe_2$ and $1T$-TaS_2, our entropy-based argument may also account for the unique presence of NTE in the former compound. These results collectively highlight the important role of lattice entropy and suggest a practical platform to delicately manipulate the electron correlation and study the exotic d^1 physics by engineering of phase(s) and temperature. The methods and insights in this paper may also be instrumental and transferrable to understand multiple CCDW phases in some other $1T$-TMD materials containing more d electrons [48].

ACKNOWLEDGMENTS

This work is supported by the National Natural Science Foundation of China (Grants No. 12047508, No. 11904350, No. 12374062, and No. 92365201), Open Research Fund Program of the State Key Laboratory of Low-Dimensional Quantum Physics (Grant No. KF202202) and Anhui Provincial Natural Science Foundation (Grant No. 2008085QA30). Part of the calculations are performed at Tianhe2-JK at Beijing Computational Science Research Center.

[1] J. Wilson, F. D. Salvo, and S. Mahajan, Charge-density waves and superlattices in the metallic layered transition metal dichalcogenides, Adv. Phys. **24**, 117 (1975).

[2] X. Liu, Y. X. Chong, R. Sharma, and J. C. S. Davis, Discovery of a Cooper-pair density wave state in a transition-metal dichalcogenide, Science **372**, 1447 (2021).

[3] B. Sipos, A. F. Kusmartseva, A. Akrap, H. Berger, L. Forró, and E. Tutiš, From Mott state to superconductivity in $1T$-TaS_2, Nat. Mater. **7**, 960 (2008).

[4] Y. Yu, F. Yang, X. F. Lu, Y. J. Yan, Y.-H. Cho, L. Ma, X. Niu, S. Kim, Y.-W. Son, D. Feng *et al.*, Gate-tunable phase transitions in thin flakes of $1T$-TaS_2, Nat. Nano **10**, 270 (2015).

[5] M. M. Ugeda, A. J. Bradley, Y. Zhang, S. Onishi, Y. Chen, W. Ruan, C. Ojeda-Aristizabal, H. Ryu, M. T. Edmonds, H.-Z. Tsai *et al.*, Characterization of collective ground states in single-layer $NbSe_2$, Nat. Phys. **12**, 92 (2016).

[6] S. Manzeli, D. Ovchinnikov, D. Pasquier, O. V. Yazyev, and A. Kis, 2D transition metal dichalcogenides, Nat. Rev. Mater. **2**, 17033 (2017).

[7] M. Calandra, Phonon-assisted magnetic Mott-insulating state in the charge density wave phase of single-layer $1T$-$NbSe_2$, Phys. Rev. Lett. **121**, 026401 (2018).

[8] H. Lin, W. Huang, K. Zhao, S. Qiao, Z. Liu, J. Wu, X. Chen, and S.-H. Ji, Scanning tunneling spectroscopic study of monolayer $1T$-TaS_2 and $1T$-$TaSe_2$, Nano Res. **13**, 133 (2020).

[9] Y. Nakata, K. Sugawara, A. Chainani, H. Oka, C. Bao, S. Zhou, P.-Y. Chuang, C.-M. Cheng, T. Kawakami, Y. Saruta *et al.*, Robust charge-density wave strengthened by electron correlations in monolayer $1T$-$TaSe_2$ and $1T$-$NbSe_2$, Nat. Commun. **12**, 5873 (2021).

[10] N. Yoshikawa, H. Suganuma, H. Matsuoka, Y. Tanaka, P. Hemme, M. Cazayous, Y. Gallais, M. Nakano, Y. Iwasa, and R. Shimano, Ultrafast switching to an insulating-like metastable state by amplitudon excitation of a charge density wave, Nat. Phys. **17**, 909 (2021).

[11] S. Qiao, X. Li, N. Wang, W. Ruan, C. Ye, P. Cai, Z. Hao, H. Yao, X. Chen, J. Wu *et al.*, Mottness collapse in $1T$-$TaS_{2-x}Se_x$ transition-metal dichalcogenide: An interplay between localized and itinerant orbitals, Phys. Rev. X **7**, 041054 (2017).

[12] D. Shin, N. Tancogne-Dejean, J. Zhang, M. S. Okyay, A. Rubio, and N. Park, Identification of the Mott insulating charge density wave state in $1T$-TaS_2, Phys. Rev. Lett. **126**, 196406 (2021).

[13] D. Lee, K.-H. Jin, F. Liu, and H. W. Yeom, Tunable Mott Dirac and kagome bands engineered on $1T$-TaS_2, Nano Lett. **22**, 7902 (2022).

[14] X. Song, L. Liu, Y. Chen, H. Yang, Z. Huang, B. Hou, Y. Hou, X. Han, H. Yang, Q. Zhang *et al.*, Atomic-scale visualization of chiral charge density wave superlattices and their reversible switching, Nat. Commun. **13**, 1843 (2022).

[15] L. Stojchevska, I. Vaskivskyi, T. Mertelj, P. Kusar, D. Svetin, S. Brazovskii, and D. Mihailovic, Ultrafast switching to a stable hidden quantum state in an electronic crystal, Science **344**, 177 (2014).

[16] I. Vaskivskyi, I. Mihailovic, S. Brazovskii, J. Gospodaric, T. Mertelj, D. Svetin, P. Sutar, and D. Mihailovic, Fast electronic resistance switching involving hidden charge density wave states, Nat. Commun. **7**, 11442 (2016).

[17] A. K. Geremew, S. Rumyantsev, F. Kargar, B. Debnath, A. Nosek, M. A. Bloodgood, M. Bockrath, T. T. Salguero, R. K. Lake, and A. A. Balandin, Bias-voltage driven switching of the charge-density-wave and normal metallic phases in $1T$-TaS_2 thin-film devices, ACS Nano **13**, 7231 (2019).

[18] K. Law and P. A. Lee, $1T$-TaS_2 as a quantum spin liquid, Proc. Natl Acad. Sci. USA **114**, 6996 (2017).

[19] M. Klanjšek, A. Zorko, R. žitko, J. Mravlje, Z. Jagličić, P. K. Biswas, P. Prelovšek, D. Mihailovic, and D. Arčon, A high-temperature quantum spin liquid with polaron spins, Nat. Phys. **13**, 1130 (2017).

[20] A. Ribak, I. Silber, C. Baines, K. Chashka, Z. Salman, Y. Dagan, and A. Kanigel, Gapless excitations in the ground state of $1T$-TaS_2, Phys. Rev. B **96**, 195131 (2017).

[21] Y. J. Yu, Y. Xu, L. P. He, M. Kratochvilova, Y. Y. Huang, J. M. Ni, L. Wang, S.-W. Cheong, J.-G. Park, and S. Y. Li, Heat transport study of the spin liquid candidate $1T$-TaS_2, Phys. Rev. B **96**, 081111(R) (2017).

[22] W.-Y. He, X. Y. Xu, G. Chen, K. T. Law, and P. A. Lee, Spinon Fermi surface in a cluster Mott insulator model on a triangular lattice and possible application to $1T$-TaS_2, Phys. Rev. Lett. **121**, 046401 (2018).

[23] H. Murayama, Y. Sato, T. Taniguchi, R. Kurihara, X. Z. Xing, W. Huang, S. Kasahara, Y. Kasahara, I. Kimchi, M. Yoshida *et al.*, Effect of quenched disorder on a quantum spin liquid state of triangular-lattice antiferromagnet $1T$-TaS_2, Phys. Rev. Res. **2**, 013099 (2020).

[24] W. Ruan, Y. Chen, S. Tang, J. Hwang, H.-Z. Tsai, R. L. Lee, M. Wu, H. Ryu, S. Kahn, F. Liou *et al.*, Evidence for quantum spin liquid behaviour in single-layer $1T$-$TaSe_2$ from scanning tunnelling microscopy, Nat. Phys. **17**, 1154 (2021).

[25] J. Dai, J. Qiao, C. Wang, L. Zhou, X. Wu, L. Liu, X. Song, F. Pang, Z. Cheng, X. Kong *et al.*, Layer sliding and twisting

induced electronic transitions in correlated magnetic 1T-$NbSe_2$ bilayers, Adv. Funct. Mater. **33**, 2302989 (2023).

[26] F. Kadijk and F. Jellinek, On the polymorphism of niobium diselenide, J. Less-Common Met. **23**, 437 (1971).

[27] X. Xi, L. Zhao, Z. Wang, H. Berger, L. Forró, J. Shan, and K. F. Mak, Strongly enhanced charge-density-wave order in monolayer $NbSe_2$, Nat. Nanotechnol. **10**, 765 (2015).

[28] X. Xi, Z. Wang, W. Zhao, J.-H. Park, K. T. Law, H. Berger, L. Forró, J. Shan, and K. F. Mak, Ising pairing in superconducting $NbSe_2$ atomic layers, Nat. Phys. **12**, 139 (2016).

[29] D. Wickramaratne, S. Khmelevskyi, D. F. Agterberg, and I. I. Mazin, Ising superconductivity and magnetism in $NbSe_2$, Phys. Rev. X **10**, 041003 (2020).

[30] Y. Nakata, K. Sugawara, R. Shimizu, Y. Okada, P. Han, T. Hitosugi, K. Ueno, T. Sato, and T. Takahashi, Monolayer 1T-$NbSe_2$ as a Mott insulator, NPG Asia Mater. **8**, e321 (2016).

[31] L. Liu, H. Yang, Y. Huang, X. Song, Q. Zhang, Z. Huang, Y. Hou, Y. Chen, Z. Xu, T. Zhang *et al.*, Direct identification of Mott Hubbard band pattern beyond charge density wave superlattice in monolayer 1T-$NbSe_2$, Nat. Commun. **12**, 1978 (2021).

[32] M. Liu, J. Leveillee, S. Lu, J. Yu, H. Kim, C. Tian, Y. Shi, K. Lai, C. Zhang, F. Giustino *et al.*, Monolayer 1T-$NbSe_2$ as a 2D-correlated magnetic insulator, Sci. Adv. **7**, eabi6339 (2021).

[33] Z.-Y. Liu, S. Qiao, B. Huang, Q.-Y. Tang, Z.-H. Ling, W.-H. Zhang, H.-N. Xia, X. Liao, H. Shi, W.-H. Mao *et al.*, Charge transfer gap tuning via structural distortion in monolayer 1T-$NbSe_2$, Nano Lett. **21**, 7005 (2021).

[34] G. Kresse and J. Hafner, *Ab initio* molecular dynamics for liquid metals, Phys. Rev. B **47**, 558 (1993).

[35] G. Kresse and J. Hafner, *Ab initio* molecular-dynamics simulation of the liquid-metal-amorphous-semiconductor transition in germanium, Phys. Rev. B **49**, 14251 (1994).

[36] G. Kresse and J. Furthmüller, Efficiency of *ab initio* total energy calculations for metals and semiconductors using a plane-wave basis set, Comput. Mater. Sci. **6**, 15 (1996).

[37] G. Kresse and J. Furthmüller, Efficient iterative schemes for *ab initio* total-energy calculations using a plane-wave basis set, Phys. Rev. B **54**, 11169 (1996).

[38] A. Liechtenstein, V. Anisimov, and J. Zaanen, Density-functional theory and strong interactions: Orbital ordering in Mott-Hubbard insulators, Phys. Rev. B **52**, R5467 (1995).

[39] S. L. Dudarev, G. A. Botton, S. Y. Savrasov, C. J. Humphreys, and A. P. Sutton, Electron-energy-loss spectra and the structural stability of nickel oxide: An LSDA+U study, Phys. Rev. B **57**, 1505 (1998).

[40] L. Cheng, S. Zhang, S. Qiao, X. Wang, L. Liu, and Z. Liu, Renormalization of the Mott gap by lattice entropy: The case of 1T-TaS_2, Phys. Rev. Res. **2**, 023064 (2020).

[41] D. Pasquier and O. V. Yazyev, Charge density wave phase, Mottness, and ferromagnetism in monolayer 1T-$NbSe_2$, Phys. Rev. B **98**, 045114 (2018).

[42] See Supplemental Material at http://link.aps.org/supplemental/10.1103/PhysRevB.108.214103 for the importance of the +U correction (Table S1 and Fig. S1); structural parameters (high-symmetric, LBS, and HBS); effects of NTE on the Mott physics (Fig. S2 and Table S2); and the two low-energy modes corresponding to the breathing of SDs in the CCDW phase of 1T-$NbSe_2$ and 1T-TaS_2 (Fig. S3).

[43] A. Togo and I. Tanaka, First principles phonon calculations in materials science, Scr. Mater. **108**, 1 (2015).

[44] Y. Zheng, X. Jiang, X.-X. Xue, X. Yao, J. Zeng, K.-Q. Chen, E. Wang, and Y. Feng, Nuclear quantum effects on the charge-density wave transition in NbX_2 (X = S, Se), Nano Lett. **22**, 1858 (2022).

[45] A. Schobert, J. Berges, E. G. C. P. van Loon, M. A. Sentef, S. Brener, M. Rossi, and T. O. Wehling, *Ab initio* electron-lattice downfolding: Potential energy landscapes, anharmonicity, and molecular dynamics in charge density wave materials, arXiv:2303.07261.

[46] L. Cheng, X. Long, X. Chen, X. Zou, and Z. Liu, Understanding the flat band in 1T-TaS_2 using a rotated basis, Phys. Rev. B **104**, L241114 (2021).

[47] G. Chen, K. R. A. Hazzard, A. M. Rey, and M. Hermele, Synthetic-gauge-field stabilization of the chiral-spin-liquid phase, Phys. Rev. A **93**, 061601(R) (2016).

[48] X. Ma, T. Dai, S. Dang, S. Kang, X. Chen, W. Zhou, G. Wang, H. Li, P. Hu, Z. He *et al.*, Charge density wave phase transitions in large-scale few-layer 1T-VTe_2 grown by molecular beam epitaxy, ACS Appl. Mater. Interfaces **11**, 10729 (2019).